AIAA JOURNAL
Vol. 30, No. 11, November 1992

Dilatation-Dissipation Corrections for Advanced Turbulence Models

David C. Wilcox*
DCW Industries, Inc., La Cañada, California 91011

This paper analyzes dilatation-dissipation based compressibility corrections for advanced turbulence models. Numerical computations verify that the dilatation-dissipation corrections devised by Sarkar and Zeman greatly improve both the k-ω and k-ϵ model predicted effect of Mach number on spreading rate. However, computations with the k-ω model also show that the Sarkar/Zeman terms cause an undesired reduction in skin friction for the compressible flat-plate boundary layer. A perturbation solution for the compressible wall layer shows that the Sarkar and Zeman terms reduce the effective von Kármán constant in the law of the wall. This is the source of the inaccurate k-ω model skin-friction predictions for the flat-plate boundary layer. The perturbation solution also shows that the k-ϵ model has an inherent flaw for compressible boundary layers that is not compensated for by the dilatation-dissipation corrections. A compressibility modification for k-ω and k-ϵ models is proposed that is similar to those of Sarkar and Zeman. The new compressibility term permits accurate predictions for the compressible mixing layer, flat-plate boundary layer, and a shock separated flow with the same values for all closure coefficients.

I. Introduction

ACCURATE prediction of hypersonic mixing in turbulent flows poses an especially challenging problem for the fluid mechanics research community. Current interest in vehicles such as the National Aerospace Plane accentuates the need for accurate numerical simulation of flow regimes unattainable in wind tunnels. Such simulations are only as good as the model for the Reynolds stresses at hypersonic speeds. Two research avenues are available for arriving at a suitable closure model: 1) developing a new model or 2) generalizing an existing low-speed model. Developing a new model is the appropriate topic of a long-range research effort while generalizing an existing model fills more immediate needs. The primary focus in this paper is the generalization of existing turbulence models.

Generalization of an existing low-speed turbulence model poses a difficult problem for a variety of reasons. There are two primary obstacles. First, many existing turbulence models fail to accurately predict effects of adverse pressure gradient for very simple attached flows and most fail to simulate accurately low-Reynolds-number phenomena. Second, of the turbulence models that apply to compressible flows, virtually all assume the Morkovin hypothesis that requires the Mach number of turbulent fluctuations to be negligible, a questionable approximation at hypersonic speeds.

The quality of the low-speed model is not the only obstacle to developing a high-speed model, however. Even if a suitable low-speed model is selected, its successful generalization for hypersonic applications requires testing against reliable experimental data. This task is nontrivial since many of the applications of great interest involve complex phenomena such as boundary-layer separation that are difficult both to measure and to simulate numerically. As a result of over two decades of computational fluid dynamics research, we are in an excellent position to apply the greatly enhanced computing power of the 1990s to the hypersonic problem. Extremely efficient numerical algorithms have been devised[1-5] that make it possible to perform separated flow computations on a machine as small as a 32-bit desktop computer. Consequently, we can now routinely modify a turbulence model and test the modification on relatively complicated flows, without the need of a super computer.

Armed with rapid numerical tools for testing a generalized turbulence model, our most important objective is to establish a solid foundation to build on. By far, the k-ϵ model[6] is the most frequently used low-speed turbulence model, where k is turbulence kinetic energy per unit mass and ϵ is the rate of dissipation of k. Almost every turbulence modeler bases his model on an equation closely resembling the ϵ equation. However, this model suffers a variety of shortcomings that make it especially unsuitable for hypersonic flows. For example, the model is very inaccurate for even the mildest of adverse pressure gradients[7,8] and is extremely difficult to integrate through the viscous sublayer. The latter point is especially important for hypersonic flows. Even at a very high Reynolds number, hypersonic boundary layers appear almost transitional wherefore viscous effects almost certainly are important. Consequently, we need a baseline turbulence model that does not use the ϵ equation.

As pointed out by Lakshminarayana,[9] the k-ω models devised by Kolmogorov,[10] Saffman,[11] and Wilcox[7,12] are the second most widely used class of models. The quantity ω is the specific dissipation rate and can be thought of as the ratio of ϵ to k. Using the ω equation in place of the ϵ equation offers two immediate advantages. First, the k-ω model is far more accurate than the k-ϵ model for incompressible boundary layers in adverse pressure gradient.[7] Second, the model equations can be integrated through the viscous sublayer with no particular difficulty.

Thus, we begin with the Wilcox k-ω model[7] and multiscale model[12] as the foundation for a new hypersonic turbulence model. As with virtually all other turbulence models, no special compressibility modifications have been made before this study. The purpose of this paper is to begin the process of generalizing the models for hypersonic flows by devising and testing suitable compressibility modifications.

In Sec. II the compressibility terms postulated by Sarkar and by Zeman are analyzed. The terms are adapted to the k-ω model, and model predictions for the compressible mixing layer, flat-plate boundary layer, and a shock-separated flow are tested. In Sec. III the compressible law of the wall implied by the modified k-ω and k-ϵ models is deduced with the Sarker

Presented as Paper 91-1785 at the AIAA 22nd Fluid Dynamics, Plasmadynamics and Lasers Conference, Honolulu, HI, June 24-26, 1991; received Dec. 5, 1991; revision received April 8, 1992; accepted for publication April 8, 1992.

*President. Associate Fellow AIAA.

compressibility term included. On the basis of these results, an improved compressibility term is postulated in Sec. IV and tested in Sec. V. Sec. VI presents a summary of and conclusions drawn from the study.

II. Compressibility Terms of Sarkar and Zeman

The appendix summarizes the equations that constitute the Wilcox k-ω two-equation model and multiscale model. Both models fail to predict the observed decrease in spreading rate for the compressible mixing layer. Focusing on the k-ϵ model, Sarkar et al.[13] and Zeman[14] have devised particularly elegant modifications to the k equation that correct the deficiency for the compressible mixing layer. By expressing the dissipation of k as the sum of solenoidal (ϵ) and dilatational (ϵ_d) components, Sarkar and Zeman argue that the total dissipation should be a function of turbulence Mach number M_t defined by

$$M_t^2 = 2k/a^2 \tag{1}$$

where a is the speed of sound. They argue that the k and ϵ equations should be as follows:

$$\rho \frac{dk}{dt} = -\rho(\epsilon + \epsilon_d) + \cdots \tag{2}$$

$$\rho \frac{d\epsilon}{dt} = -C_{\epsilon 2}\rho\epsilon^2/k + \cdots \tag{3}$$

where $C_{\epsilon 2}$ is a closure coefficient. Only the dissipation terms appear explicitly in Eqs. (2) and (3) since no changes occur in any other terms. It should be noted that both Sarkar and Zeman postulate that the equation for ϵ is unaffected by compressibility. The dilatational, or compressible, dissipation is further assumed to be proportional to ϵ; thus, we can write

$$\epsilon_d = \xi^* F(M_t)\epsilon \tag{4}$$

where ξ^* is a closure coefficient and $F(M_t)$ is a prescribed function of M_t. The Sarkar and Zeman formulations differ in the value of ξ^* and functional form of $F(M_t)$. To implement the Sarkar or Zeman modification in the k-ω model, we begin by making the formal change of variables given by $\epsilon = \beta^*\omega k$. This tells us immediately that

$$\rho \frac{d\omega}{dt} = \frac{\rho}{\beta^* k}\left(\frac{d\epsilon}{dt} - \frac{\epsilon}{k}\frac{dk}{dt}\right) \tag{5}$$

Consequently, a compressibility term must appear in the ω equation as well as in the k equation. Thus, as seen in Eqs. (A4) and (A5) in Appendix A, the Sarkar/Zeman compressibility modifications correspond to letting closure coefficients β and β^* vary with M_t. In terms of ξ^* and the compressibility function $F(M_t)$, β and β^* are as follows:

$$\beta^* = \beta_0^*[1 + \xi^* F(M_t)] \tag{6}$$

$$\beta = \beta_0 - \beta_0^* \xi^* F(M_t) \tag{7}$$

where β_0^* and β_0 are the corresponding incompressible values of β^* and β. Finally, the values of ξ^* and $F(M_t)$ for the Sarkar and Zeman models are as follows.

Sarkar's model:

$$\xi^* = 1 \qquad F(M_t) = M_t^2 \tag{8}$$

Zeman's model

$$\xi^* = 3/4$$

$$F(M_t) = [1 - \exp\{-\tfrac{1}{2}(\gamma + 1)(M_t - M_{t0})^2/\Lambda^2\}] \times H(M_t - M_{t0}) \tag{9}$$

where γ is specific heat ratio and $H(x)$ is the Heaviside step function. Zeman[14] recommends using $M_{t0} = 0.10[2/(\gamma + 1)]^{1/2}$ and $\Lambda = 0.60$ for free shear flows. For boundary layers, their values must increase to $M_{t0} = 0.25[2/(\gamma + 1)]^{1/2}$ and $\Lambda = 0.66$. Zeman uses a different set of closure coefficients for boundary layers because he postulates that they depend on the kurtosis, $\langle u'^4\rangle/\langle u'^2\rangle$. The kurtosis is presumed to be different for free shear flows than for boundary layers. Although this is probably true, it is not much help for two-equation or second-order closure models since such models only compute double correlations with closure approximations for triple correlations. Quadruple correlations such as $\langle u'^4\rangle$ are beyond the scope of these models. Consequently, the Zeman model is effectively a zonal model in the context of two-equation and second-order closure models.

Using the k-ϵ model, Sarkar and Zeman tested their compressibility modification for the effect of Mach number on the mixing layer. Both have been able to predict the measured reduction in spreading rate with increasing freestream Mach number. As the first step in this study, using the k-ω model, we have tested the Sarkar and Zeman compressibility modifications for the compressible mixing layer and the compressible flat-plate boundary layer. Additionally, we have tested the Sarkar compressibility term for a shock-separated flow.

A. Compressible Mixing Layer

The first application is for the compressible mixing layer. Mixing occurs between a supersonic stream and a quiescent fluid with constant total temperature. The equations of motion for the k-ω model have been transformed to similarity form for the far field and integrated using an implicit time-marching procedure. The program used to solve the equations of motion, known as MIXER,[15] implements the Rubel-Melnik[16] transformation and implicit Crank-Nicholson differencing. The Rubel-Melnik transformation obviates the need to cluster grid points in regions of rapid change and accurately resolves turbulent/nonturbulent interfaces. To ensure numerically accurate solutions, the grid point number was varied from 50 to 500. The use of 300 grid points is sufficient to achieve spreading rates accurate to four significant figures. All computations have been done with 300 equally spaced grid points.

Figure 1 compares the computed and measured[17] spreading rate C_δ. The spreading rate is defined as the difference between the values of y/x at the points where the square of the velocity is within 10% of the freestream value. The quantity $C_{\delta 0}$ denotes the incompressible spreading rate, and M_c is convective Mach number:

$$M_c = \frac{U_1 - U_2}{a_1 + a_2} \tag{10}$$

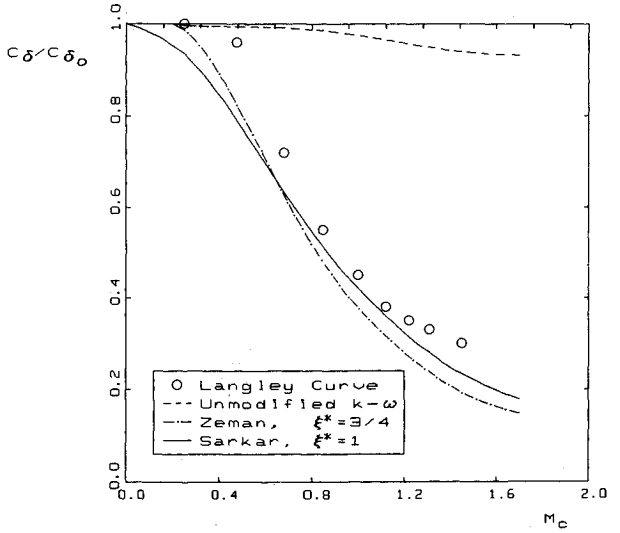

Fig. 1 Comparison of computed and measured spreading rate for a compressible mixing layer.

Since $U_2 = 0$, Eq. (10) simplifies to

$$M_c = \frac{M_1}{1 + [1 + \tfrac{1}{2}(\gamma - 1)M_1^2]^{1/2}} \tag{11}$$

As shown, the unmodified k-ω model fails to predict a significant decrease in spreading rate as the Mach number increases. In contrast, both the Sarkar and Zeman modifications yield much closer agreement between computed and measured spreading rate.

B. Compressible Flat-Plate Boundary Layer

We turn now to the adiabatic wall flat-plate boundary layer. The equations of motion for the k-ω model have been solved with a compressible boundary-layer program known as EDDYBL[16] that uses the Blottner[18] variable-grid method. In many prior applications this program has been shown to yield grid-independent solutions using 100 grid points. All computations in this study have been done using 150 grid points. Computation has been initiated at the plate leading edge, continued through transition from laminar to turbulent flow, and terminated when momentum thickness Reynolds number Re_θ reaches 10^4, i.e., the value recommended by Kline et al.[17] for computing compressible flat-plate c_f.

Figure 2 compares computed skin friction c_f with a correlation of measured values for freestream Mach number between 0 and 5. As shown, the unmodified model virtually duplicates measured skin friction. In contrast, the Sarkar compressibility modification yields a value for c_f at Mach 5 that is 18% lower than the value computed with $\xi^* = 0$.

When $M_{t0} = 0.10[2/(\gamma + 1)]^{1/2}$ and $\Lambda = 0.60$ in Zeman's model are used, computed c_f at Mach 5 is 15% smaller than the value obtained with the unmodified model. Increasing M_{t0} and Λ to $0.25[2/(\gamma + 1)]^{1/2}$ and 0.66, respectively, eliminates this discrepancy. However, using this large a value for M_{t0} for the mixing layer results in discrepancies in excess of 100% between computed and measured spreading rate.

C. Shock-Separated Flow

The final application is to a flow that includes boundary-layer separation induced by interaction with a shock wave. Specifically, we consider Mach 2.79 flow into a 20 deg compression corner as documented by Settles et al.[19] Computations have been done with a two-dimensional Navier-Stokes program known as EDDY2C[20] that uses MacCormack's Gauss-Seidel-based algorithm.[5]

The finite difference mesh consists of parallelograms with uniform spacing in the streamwise direction. Finite difference cells are stretched in a geometric progression in the y direction. To guarantee mesh independence, we have used grids consisting of 40×35, 80×45, and 120×60 (streamwise times normal) points. The value of y^+ at the first grid point above the surface lies between 0.1 and 0.5 throughout the finest grid. In terms of the initial boundary-layer thickness δ_0, all three finite difference meshes extend $8\delta_0$ in the streamwise direction and $6\delta_0$ in the y direction, with the upstream boundary $2\delta_0$ ahead of the corner. The computations require 150 time steps to reach steady flow conditions. Computing time required for the finest mesh is 3 h and 3.5 h on a 25 MHz 80486/4167-based microcomputer for the k-ω model and the multiscale model, respectively. Computed separation-bubble length changes by $< 0.3\%$ between the 80×45 and 120×60 meshes.

Figure 3 compares computed and measured surface pressure p_w and skin friction for the computation, including results for the unmodified k-ω model ($\xi^* = 0$) and for the k-ω model with Sarkar's compressibility term using $\xi^* = 1$. Computations have not been performed using Zeman's term. Such computations seem pointless considering the similarity in the results obtained with Sarkar's and Zeman's models for the mixing layer and flat-plate boundary layer.

The most notable difference is in separation-bubble size. Without the Sarkar term, the separation bubble length is

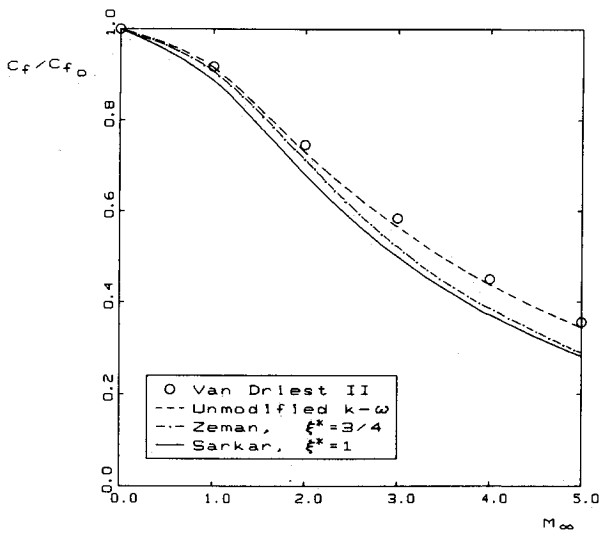

Fig. 2 Comparison of computed and measured skin friction for a compressible flat-plate boundary layer.

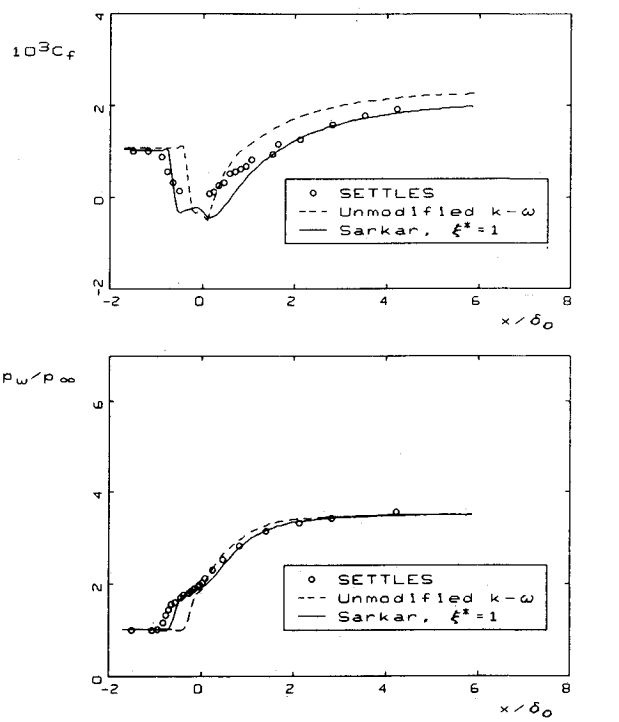

Fig. 3 Comparison of computed and measured skin friction and surface pressure for Mach 2.79 flow into a 20-deg compression corner.

$0.52\delta_0$. When the Sarkar term is included, the bubble length increases to $1.21\delta_0$. Close agreement between computed and measured surface pressure distributions shows that using the Sarkar compressibility term more closely simulates the experimental flowfield that is very sensitive to separation-bubble size. Using the Sarkar term improves the overall solution because it yields a larger separation bubble.

Considering all of the applications, we have shown that the Sarkar and Zeman compressibility terms offer a promising, but imperfect, method of improving two-equation turbulence model predictions for compressible flows. On one hand, both compressibility terms applied to the k-ω and the k-ϵ models reproduce the observed reduction of the compressible mixing layer's spreading rate with increasing Mach number. Additionally, Sarkar's compressibility term reduces discrepancies between computed and measured separation-bubble size for

the one flow with shock-induced separation that we have considered. On the other hand, both compressibility terms yield inferior predictions for the adiabatic-wall flat-plate boundary layer. This explains why the skin friction is somewhat low in the recovery region downstream of reattachment for the compression corner case (Fig. 3). The purpose of the following sections is to determine why the modification is inconsistent and to develop an improved compressibility term that can be used for all of the flows considered, with the same values of all closure coefficients.

III. Compressible Law of the Wall

Although the Sarkar and Zeman compressibility terms improve model predictions for the compressible mixing layer, they appear to have an undesirable effect on the compressible flat-plate boundary layer. In this section we examine model-predicted, compressible wall-layer structure. The results are particularly illuminating and clearly demonstrate why these compressibility terms adversely affect boundary-layer predictions.

A. Perturbation Solution

By definition, the wall layer is the region sufficiently close to the solid boundary for neglect of convective terms and far enough distant for molecular diffusion terms to be dropped. The following analysis closely parallels the work of Saffman and Wilcox.[21] The most important difference between the solution here and that of Saffman and Wilcox is in retention of terms of order M_t^2. In the wall layer, the equations of motion based on the k-ω model simplify to the following.

$$\mu_T \frac{du}{dy} = \rho_w u_\tau^2 \tag{12}$$

$$\mu_T \frac{d}{dy}\left[\frac{C_p T}{Pr_T} + \tfrac{1}{2}u^2 + \sigma^* k\right] = -q_w \tag{13}$$

$$\sigma^* \frac{d}{dy}\left[\mu_T \frac{dk}{dy}\right] + u_T\left(\frac{du}{dy}\right)^2 - \beta^* \rho \omega k = 0 \tag{14}$$

$$\sigma \frac{d}{dy}\left[\mu_T \frac{d\omega}{dy}\right] + \alpha\rho\left(\frac{du}{dy}\right)^2 - \beta\rho\omega^2 = 0 \tag{15}$$

$$\rho T = \rho_w T_w \tag{16}$$

The quantity u_τ is the friction velocity defined as $(\tau_w/\rho_w)^{1/2}$, where τ_w is the surface shear stress and ρ_w the density at the surface. Also, T_w is the surface temperature, q_w the surface heat flux, C_p, the specific heat at constant pressure and y is the distance from the surface. All other symbols and notation are defined in Appendix A.

Following Saffman and Wilcox, we change independent variables from y to u. Consequently, derivatives transform according to

$$\mu_T \frac{d}{dy} = \mu_T \frac{du}{dy}\frac{d}{du} = \rho_w u_\tau^2 \frac{d}{du} \tag{17}$$

With this change of dependent variables, we replace Eqs. (13-15) by the following:

$$\frac{d}{du}\left[\frac{C_p T}{Pr_T} + \frac{1}{2}u^2 + \sigma^* k\right] = \frac{-q_w}{\rho_w u_\tau^2} \tag{18}$$

$$\sigma^* \frac{d^2k}{du^2} + 1 - \frac{\beta^* \rho^2 k^2}{\rho_w^2 u_\tau^4} = 0 \tag{19}$$

$$\sigma \frac{d^2\omega}{du^2} + \alpha \frac{\omega}{k} - \frac{\beta \rho^2 k \omega}{\rho_w^2 u_\tau^4} = 0 \tag{20}$$

Integrating Eq. (18) yields the temperature, and hence the density, as a function of velocity and Mach number based on friction velocity $M_\tau \equiv u_\tau/a_w$:

$$\frac{T}{T_w} = \frac{\rho_w}{\rho} = 1 - (\gamma - 1) Pr_T M_\tau^2 \left[\frac{1}{2}\left(\frac{u}{u_\tau}\right)^2 + \left(\frac{q_w}{\rho_w u_\tau^3}\right)\left(\frac{u}{u_\tau}\right) + \sigma^*\left(\frac{k}{u_\tau^2}\right)\right] \tag{21}$$

Then, following Saffman and Wilcox, we assume a solution of the following form:

$$\rho k = \Gamma \rho_w u_\tau^2 \tag{22}$$

where Γ is a constant to be determined. Substituting Eqs. (21) and (22) into Eq. (19) and noting that $M_t^2 = 2\Gamma M_\tau^2$ leads to the following quartic equation for Γ:

$$\beta_0^*[1 + 2\xi^* M_\tau^2 \Gamma][1 + (\gamma - 1) Pr_T \sigma^* M_\tau^2 \Gamma]\Gamma^2 = 1 \tag{23}$$

As can easily be verified, when $M_\tau^2 \ll 1$, the asymptotic solution for Γ is

$$\Gamma = \frac{1}{\sqrt{\beta_0^*}} - \left[\frac{\xi^* + \tfrac{1}{2}(\gamma - 1) Pr_T \sigma^*}{\beta_0^*}\right] M_\tau^2 + \cdots \tag{24}$$

Finally, in terms of Γ, Eq. (20) simplifies to the following equation:

$$\sigma \frac{d^2\omega}{du^2} + \{\alpha - [\beta_0 - 2\beta_0^* \xi^* M_\tau^2 \Gamma]\Gamma^2\} \frac{\rho\omega}{\rho_w u_\tau^2 \Gamma} = 0 \tag{25}$$

Combining Eqs. (21) and (22) yields the density as a function of velocity and Γ:

$$\frac{\rho_w}{\rho} = \frac{1 - (\gamma - 1) Pr_T M_\tau^2 [\tfrac{1}{2}(u/u_\tau)^2 + (q_w/\rho_w u_\tau^3)(u/u_\tau)]}{1 + (\gamma - 1) Pr_T \sigma^* \Gamma M_\tau^2} \tag{26}$$

Equation (26) assumes a more compact form if we introduce the freestream velocity U_∞. A bit more algebra yields

$$\frac{\rho_w}{\rho} = \frac{1 + Bv - A^2 v^2}{1 + (\gamma - 1) Pr_T \sigma^* \Gamma M_\tau^2} \tag{27}$$

where

$$\begin{aligned} v &= u/U_\infty \\ A^2 &= \tfrac{1}{2}(\gamma - 1) Pr_T M_\infty^2 (T_\infty/T_w) \\ B &= -Pr_T q_w U_\infty/(C_p T_w \tau_w) \end{aligned} \tag{28}$$

Using Eqs. (24), (27), and (28), and retaining terms up to $\mathcal{O}(M_t^2)$, Eq. (25) assumes the following form:

$$\frac{d^2\omega}{dv^2} - K^2\left(\frac{U_\infty}{u_\tau}\right)^2 [1 + Bv - A^2 v^2]^{-1}\omega = 0 \tag{29}$$

where the constant K is defined by

$$K^2 = \kappa^2 - [\xi^*(2 + \alpha + \beta_0/\beta_0^*)/\sigma + \tfrac{1}{2}(\gamma - 1) Pr_T \sigma^*(3\alpha - \beta_0/\beta_0^*)/\sigma] M_\tau^2 + \cdots \tag{30}$$

and κ is the von Kármán constant. Because $U_\infty/u_\tau \gg 1$, we can use the WKBJ method[22] to solve Eq. (29). Noting that ω decreases as u/U_∞ increases, the asymptotic solution for ω is as follows:

$$\omega \sim C[1 + Bv - A^2 v^2]^{1/4} \exp[-Ku^*/u_\tau] \tag{31}$$

where C is a constant of integration, and u^* is defined by

$$\frac{u^*}{U_\infty} = \frac{1}{A} \sin^{-1}\left(\frac{2A^2 v - B}{\sqrt{B^2 + 4A^2}}\right) \tag{32}$$

Combining Eqs. (12), (22), and (31), we can relate velocity and distance from the surface:

$$\int [1 + Bv - A^2v^2]^{-1/4} \exp[Ku^*/u_\tau]\, dv \sim Cy/(\Gamma U_\infty) \quad (33)$$

We use Watson's lemma to generate the asymptotic expansion of the integral in Eq. (33) as $U_\infty/u_\tau \to \infty$. Hence,

$$[1 + Bv - A^2v^2]^{1/4} \exp[Ku^*/u_\tau] \sim KCy/(\Gamma u_\tau) \quad (34)$$

Finally, we set the constant of integration $C = \Gamma u_\tau^2/(K\nu_w)$. Taking the natural log of Eq. (34), we conclude that

$$\frac{u^*}{u_\tau} \sim \frac{1}{K} \log \frac{u_\tau y}{\nu_w} + \left[\text{const} + \frac{1}{K} \log \left(\frac{\rho}{\rho_w} \right)^{1/4} \right] \quad (35)$$

Equation (35) is very similar to the compressible law of the wall deduced by van Driest.[23] There are two ways in which Eq. (35) differs from the van Driest law. 1) The effective variation in the "constant" term with (ρ/ρ_w) is a minor deviation inherent to the k-ω model. As shown by Wilcox and Traci,[24] the effect is slight. For example, in a Mach 5 adiabatic wall flat-plate boundary layer, the deviation in the constant is < 0.5 in a typical wall layer. This small a deviation is of little consequence. 2) The effective von Kármán constant K varies with M_τ according to Eq. (30). In terms of the k-ω model closure coefficients, Eq. (30) becomes (for $M_\tau \ll 1$)

$$K^2 \sim \kappa^2[1 - (40.29\xi^* + 0.87)M_\tau^2 + \cdots] \quad (36)$$

Table 1 summarizes results obtained in the boundary-layer computations of Sec. II.B for the unmodified k-ω model ($\xi^* = 0$) and for the k-ω model with the Sarkar compressibility term ($\xi^* = 1$). The value of K for the unmodified model deviates from the von Kármán constant, $\kappa = 0.41$, by $< 0.12\%$ for freestream Mach numbers between 0 and 5. In contrast, when $\xi^* = 1$, the deviation is as much as 5.10%. This large of a deviation in the effective von Kármán constant is consistent with the observed differences between computed and measured skin friction.

To see why a small perturbation in κ corresponds to a larger perturbation in c_f, differentiate the law of the wall with respect to κ. Noting that $c_f = \frac{1}{2}u_\tau^2/U_\infty^2$, a little algebra shows that

$$\frac{dc_f}{d\kappa} \approx \frac{2}{\kappa} c_f \quad (37)$$

Thus, we should expect $\Delta c_f/c_f$ to be double the value of $\Delta\kappa/\kappa$. The numerical results indicate somewhat larger differences in c_f, but the trend is clear. Inspection of computed velocity profiles verifies that the effective von Kármán constant decreases with increasing M_τ^2 in the manner indicated by Eq. (36).

B. Comments on the k-ϵ Model

Most of the analysis of the preceding subsection holds for the k-ϵ model. The only significant difference is in the ϵ equation:

$$\sigma_\epsilon^{-1} \frac{d}{dy} \left[\mu_T \frac{d\epsilon}{dy} \right] + C_\mu C_{\epsilon 1} \rho k \left(\frac{du}{dy} \right)^2 - \frac{C_{\epsilon 2} \rho \epsilon^2}{k} = 0 \quad (38)$$

Table 1 Effective von Kármán constant

M_∞	$M_\tau \mid \xi^* = 0$	K	$M_\tau \mid \xi^* = 1$	K
0	0	0.410	0	0.410
1	0.032	0.410	0.031	0.402
2	0.048	0.410	0.046	0.392
3	0.052	0.410	0.049	0.389
4	0.050	0.410	0.046	0.392
5	0.048	0.410	0.043	0.394

In Eq. (38), $C_{\epsilon 1}$, $C_{\epsilon 2}$, and C_μ are the standard closure coefficients that appear in the k-ϵ model. Also, the k-ω model's closure coefficients σ and σ^* are replaced by σ_ϵ^{-1} and σ_k^{-1}, respectively. Equations (22), (24), and (27) are still valid for the turbulence kinetic energy and density, provided σ^* is replaced by σ_k^{-1}. The transformed equation for ϵ assumes the following form:

$$\frac{d^2\epsilon}{dv^2} - K_\epsilon^2 \left(\frac{U_\infty}{u_\tau} \right)^2 [1 + Bv - A^2v^2]^{-1}\epsilon = 0 \quad (39)$$

where the constant K_ϵ is defined by

$$K_\epsilon^2 = \kappa^2 - [\xi^*(C_{\epsilon 1} + C_{\epsilon 2})\sigma_\epsilon + \tfrac{1}{2}(\gamma - 1)Pr_T \sigma k^{-1}(3C_{\epsilon 1} - C_{\epsilon 2})\sigma_\epsilon]M_\tau^2 + \cdots \quad (40)$$

In arriving at Eq. (40), we follow Patel et al.[25] and make the assumption that the k-ϵ model's closure coefficients are related by

$$\kappa^2 = \sigma_\epsilon C_\mu^{1/2}(C_{\epsilon 2} - C_{\epsilon 1}) \quad (41)$$

The asymptotic solution for ϵ is

$$\epsilon \sim C[1 + Bv - A^2v^2]^{1/4} \exp[-Ku^*/u_\tau] \quad (42)$$

Velocity and distance from the surface are related by

$$\int [1 + Bv - A^2v^2]^{3/4} \exp[Ku^*/u_\tau]\, dv \sim C_0 y \quad (43)$$

where C_0 is a constant of integration. Consequently, Eq. (34) is replaced by

$$[1 + Bv - A^2v^2]^{5/4} \exp[Ku^*/u_\tau] \sim C_1 y \quad (44)$$

where C_1 is another constant of integration. Finally, the law of the wall for the k-ϵ model is

$$\frac{u^*}{u_\tau} \sim \frac{1}{K_\epsilon} \log \left(\frac{u_\tau y}{\nu_w} \right) + \left[\text{const} + \frac{1}{K_\epsilon} \log \left(\frac{\rho}{\rho_w} \right)^{5/4} \right] \quad (45)$$

If we use the closure coefficients for the standard k-ϵ model, i.e., $C_{\epsilon 1} = 1.45$, $C_{\epsilon 2} = 1.92$, $C_\mu = 0.09$, $\sigma_\epsilon = 1.3$, and $\sigma_k = 1.0$, Eq. (40) simplifies to

$$K_\epsilon^2 \sim \kappa^2[1 - (23.92\xi^* + 3.07)M_\tau^2 + \cdots] \quad (46)$$

There are two points worthy of note: 1) With $M_\tau = 0.05$, K_ϵ differs from κ by 0.5 and 3.5% for $\xi^* = 0$ and 1, respectively. Thus, the Sarkar compressibility term has a somewhat smaller effect on κ for the k-ϵ model relative to the effect on κ for the k-ω model. 2) The exponent in the constant term is 5/4, compared to 1/4 for the k-ω model. As shown by Wilcox and Traci,[24] this large of an exponent has a much stronger effect on skin friction than the modification to κ. In a Mach 5, adiabatic wall flat-plate boundary layer, the deviation in the constant is as large as 2.5. Such a large deviation corresponds to a $> 20\%$ reduction in skin friction. This is consistent with the recent work by Huang et al.[26] that shows how poorly the k-ϵ model performs for compressible boundary layers. Since $\rho/\rho_w > 1$ for all but strongly cooled walls, its effect is to increase the constant in the law of the wall with a corresponding decrease in c_f. The Sarkar and Zeman terms will thus amplify this inherent deficiency of the k-ϵ model.

To put these results in proper perspective, we must not lose sight of the fact that the k-ϵ model requires either the use of wall functions or viscous damping functions to calculate wall-bounded flows. If these functions have an effect that persists well into the wall layer, it may be possible to suppress the k-ϵ model's inherent flaws at low Reynolds numbers. However,

the perturbation analysis shows that such a model will not be asymptotically consistent with the compressible law of the wall in the limit of infinite Reynolds number. In effect, such a model would have compensating errors that may fortuitously yield reasonably close agreement with the law of the wall at low Reynolds numbers.

As a final comment, if we had used $\rho\epsilon$ as the dependent variable in Eq. (38) in place of ϵ, the exponent 5/4 in Eq. (45) would be reduced to 1/4. Presumably, this change would improve k-ϵ model predictions for compressible boundary layers. The effect of this rescaling on the mixing layer is unclear.

IV. Improved Compressibility Term

Based on the analysis in Sec. IV, neither the Sarkar nor the Zeman compressibility term is completely satisfactory. In this section we retain the notion that the dilatation dissipation must be accounted for in a compressible flow and that it depends on turbulence Mach number. Inspection of the magnitude of the turbulence Mach number in mixing layers and boundary layers shows that all that is needed is a new functional dependence of ϵ_d on M_t.

A. Formulation

On one hand, the preceding section demonstrates why the Sarkar compressibility term causes a decrease in skin friction. Clearly, the Zeman term causes a similar decrease for essentially the same reason. On the other hand, inspection of Table 2 shows why the Sarkar term improves predictions for the mixing layer.

The unmodified k-ω model predicts peak values of M_t in the mixing layer that are roughly twice the values in the boundary layer for the same freestream Mach number. Using the Sarkar compressibility term reduces $(M_t)_{\max}$ by about one-third for the mixing layer when $M_\infty \geq 2$. Even with this much reduction, $(M_t)_{\max}$ for the mixing layer remains higher than the largest value of $(M_t)_{\max}$ in the boundary layer all the way up to Mach 5.

For Mach 1 the Sarkar term reduces mixing layer spreading rate below measured values (Fig. 1). Zeman's term predicts a somewhat larger spreading rate at Mach 1, mainly because of the lag in Zeman's model. That is, Zeman postulates that the compressibility effect is absent for $M_t < M_{t0}$. Zeman's lag also yields smaller differences between computed and measured boundary-layer skin friction at lower Mach numbers (see Fig. 2).

These observations suggest that an improved compressibility term can be devised by extending Zeman's lag to a larger value of M_t. Because of its relative simplicity, we stay with Sarkar's functional form and postulate the following alternative to Eqs. (8) and (9) with $H(x)$ again denoting the Heaviside step function.

New model:

$$\xi^* = 3/2, \qquad M_{t0} = 1/4$$
$$F(M_t) = [M_t^2 - M_{t0}^2]\, H(M_t - M_{t0}) \tag{47}$$

B. Applications

In this round of applications we use both the k-ω model and the multiscale model. Figure 4 compares the computed and the measured spreading rate for a compressible mixing layer. Computed and measured spreading rates are even closer than for the Sarkar and Zeman terms, most notably for Mach numbers between 0 and 2. The values of ξ^* and M_{t0} given in Eq. (47) have been selected to guarantee close agreement.

Table 2 Maximum turbulence Mach number $(M_t)_{\max}$

	Boundary layer		Mixing layer	
M_∞	$\xi^*=0$	$\xi^*=1$	$\xi^*=0$	$\xi^*=1$
0	0	0	0	0
1	0.061	0.061	0.180	0.159
2	0.114	0.107	0.309	0.227
3	0.149	0.135	0.384	0.245
4	0.174	0.154	0.424	0.254
5	0.191	0.171	0.453	0.266

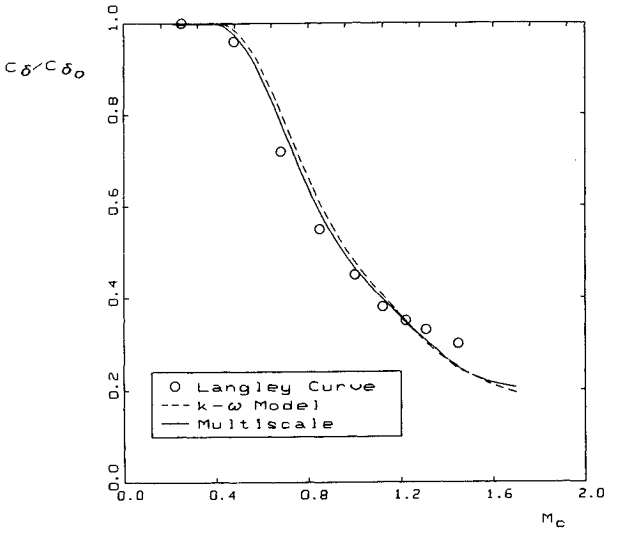

Fig. 4 Comparison of computed and measured spreading rate for a compressible mixing layer.

Figure 5 compares computed and measured skin friction for an adiabatic wall flat-plate boundary layer. As shown, the new compressibility term has an almost negligible effect for the entire range of Mach numbers considered.

Figure 6 shows results obtained for the shock-separated flow considered in Sec. II.C. The k-ω model with the new compressibility term yields a separation bubble of length $0.62\delta_0$. Although the separation bubble is slightly larger than that obtained with no compressibility term, discrepancies between computed and measured c_f and p_w are large. In suppressing the undesirable distortion of flat-plate boundary-layer skin friction, we have reduced the effectiveness of the dilatational-dissipation contribution to increased length of the separation bubble. Multiscale model results are in closer agreement with measurements, especially the size of the separation bubble, which is predicted to have a length of $1.12\delta_0$. Differences between computed and measured c_f and p_w are within engineering accuracy for the 20 deg compression corner.

The ineffectiveness of dilatation-dissipation on the k-ω model for this compression corner flow is consistent with the physics of shock-separated flows as described by Wilcox.[27] That is, these results are consistent with the notion that the Boussinesq approximation inherent in all two-equation turbulence models is inadequate for separated flows. The multiscale model computes the Reynolds stress directly rather than using the Boussinesq approximation. As shown by Wilcox,[27] the multiscale model's Reynolds shear stress grows less rapidly than the k-ω model's shear stress near a separation point. The smaller shear stress results in less resistance to reverse flow and consequently yields a larger separation bubble. Assuming that this is an accurate physical description of shock-separated flows, dilatation-dissipation should not be expected to improve two-equation model predictions for such flows. Thus, the enhanced separation-bubble length attending use of Sarkar's model (Fig. 3) may simply be a case of compensating errors.

Note that multiscale model computations have been performed with the closure coefficient $\tilde{\xi} = 0$, which suppresses the Reynolds' rotation term.[28] When this term is included, the mixing layer and flat-plate boundary layer results are essentially unchanged. However, the combination of the new compressibility term and the Reynolds rotation term yields separation bubbles about twice the size of those obtained using the compressibility term alone. Although the original multiscale

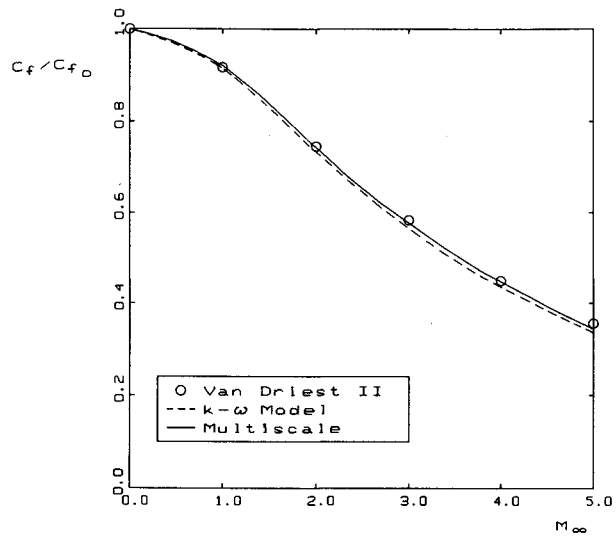

Fig. 5 Comparison of computed and measured skin friction for a compressible flat-plate boundary layer.

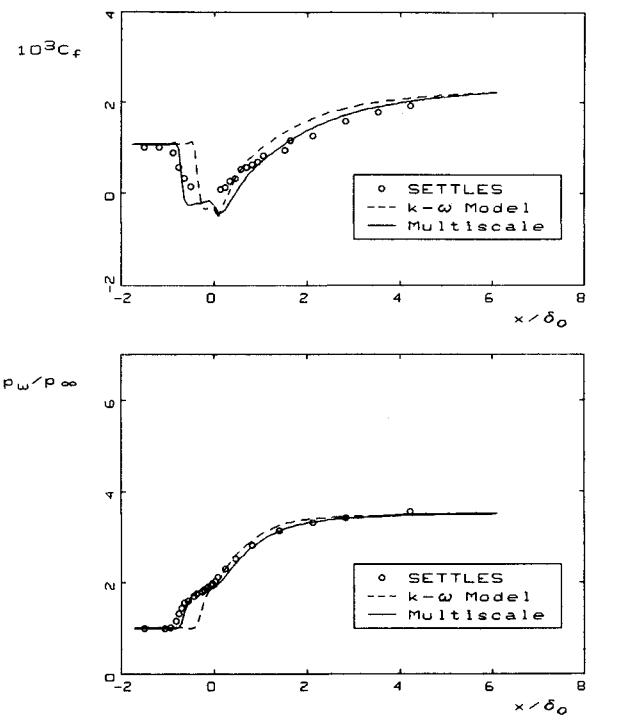

Fig. 6 Comparison of computed and measured skin friction and surface pressure for Mach 2.79 flow into a 20-deg compression corner.

model (i.e., $\xi^* = 0$ and $\hat{\xi} = 1$) yields an excellent solution, dropping the Reynolds' rotation further strengthens the case that the Boussinesq approximation is unsuitable for computing separated flows. That is, the only difference between the results shown in Fig. 6 is in the way the Reynolds stresses are computed. When $\hat{\xi} \neq 0$, we have an additional difference that does, in fact, tend to increase separation bubble length. Although results are still imperfect, at present the multiscale model with the new compressibility term appears to be the best bet for compressible-flow applications. The increase in computing time for the multiscale model relative to the k-ω model is typically ~ 20% for separated flow computations like the one performed in this study.

Summary and Conclusions

The goals of this research have been twofold. The short-term goal is to devise straightforward modifications that mimic leading-order hypersonic flow phenomena with the k-ω and multiscale models. The long-term goal is to lay the foundation for a more comprehensive analysis that will lead to a new model. This paper has focused almost exclusively on the first goal.

Results presented in Sec. II show that neither the Sarkar nor the Zeman compressibility term is completely satisfactory for both the compressible mixing layer and wall-bounded flows. The perturbation solution of Sec. III demonstrates why Sarkar's term (and, to a lesser extent, Zeman's term) causes an unwanted decrease in skin friction for the flat-plate boundary layer. The decrease is especially noticeable for the k-ω model, which accurately predicts the effect of Mach number on the flat-plate boundary layer with no compressibility corrections. The compressibility corrections cause a decrease in the effective von Kármán constant, which yields the unwanted decrease in skin friction. The effect is less noticeable with the k-ϵ model. However, for the k-ϵ model, the constant in the law of the wall varies with density ratio in a nontrivial manner. The reduction in the effective von Kármán constant further aggravates this inconsistency with the law of the wall.

Based on this analysis, we have combined Sarkar's especially simple functional dependence of dilatational dissipation on turbulence Mach number with Zeman's lag effect to produce a compressibility term [see Eq. (47)] that yields reasonably accurate predictions for all of the flows considered, with no change in the values of the closure coefficients.

Acknowledgments

This research was supported by the U.S. Army Research Office and the NASA Langley Research Center under Contract DAAL03-89-C-0032; Thomas Doligalski and Julius Harris were Contract Monitors.

Appendix: Turbulence Model Equations

For general compressible turbulent fluid flow, the complete sets of equations that constitute the Wilcox k-ω two-equation model[7] and multiscale model[12] are written in terms of Favre[29] mass-averaged quantities as follows.

Conservation of mass, momentum and energy:

$$\frac{\partial \rho}{\partial t} + \frac{\partial}{\partial x_j}(\rho u_j) = 0 \tag{A1}$$

$$\frac{\partial}{\partial t}(\rho u_i) + \frac{\partial}{\partial x_j}(\rho u_j u_i) = \frac{\partial}{\partial x_j}[-p\delta_{ji} + \hat{\tau}_{ji}] \tag{A2}$$

$$\frac{\partial}{\partial t}(\rho E) + \frac{\partial}{\partial x_j}(\rho u_j H) = \frac{\partial}{\partial x_j}\left[\hat{\tau}_{ji}u_i - q_j + (\mu + \sigma^*\mu_T)\frac{\partial k}{\partial x_j}\right] \tag{A3}$$

where t is time, x_i the position vector, u_i the velocity, ρ the density, p the pressure, μ the molecular viscosity, $\hat{\tau}_{ij}$ the sum of molecular and Reynolds stress tensors, and q_j the sum of molecular and turbulence heat flux vectors. In Eq. (A3), the quantities $E = \hat{e} + k + \frac{1}{2}u_i u_i$ and $H = h + k + \frac{1}{2}u_i u_i$ are total energy and total enthalpy, respectively, with $h = \hat{e} + p/\rho$; $\hat{e}$ and h denote internal energy and enthalpy, respectively. Also, δ_{ij} is the Kronecker delta, and k is the turbulence kinetic energy determined by the following equations.

Turbulence kinetic energy, specific dissipation rate:

$$\frac{\partial}{\partial t}(\rho k) + \frac{\partial}{\partial x_j}(\rho u_j k) = \tau_{ij}\frac{\partial u_i}{\partial x_j} - \beta^*\rho\omega k + \frac{\partial}{\partial x_j}\left[(\mu + \sigma^*\mu_T)\frac{\partial k}{\partial x_j}\right] \tag{A4}$$

$$\frac{\partial}{\partial t}(\rho\omega) + \frac{\partial}{\partial x_j}(\rho u_j \omega) = \alpha\frac{\omega}{k}\tau_{ij}\frac{\partial u_i}{\partial x_j} - \beta\rho\omega[\omega + \hat{\xi}\,|2\Omega_{mn}\Omega_{nm}|^{1/2}] + \frac{\partial}{\partial x_j}\left[(\mu + \sigma\mu_T)\frac{\partial \omega}{\partial x_j}\right] \tag{A5}$$

where ω is the specific dissipation rate, τ_{ij} the Reynolds stress tensor, and μ_T the eddy viscosity. The parameters α, β, β^*, σ, σ^*, and $\hat{\xi}$ are closure coefficients whose values are given in the following. We close the system of equations as follows.

Constitutive relations:

$$\hat{\tau}_{ij} = 2\mu\left[S_{ij} - \frac{1}{3}\frac{\partial u_k}{\partial x_k}\delta_{ij}\right] + \tau_{ij} \tag{A6}$$

$$q_j = -\left[\frac{\mu}{Pr_L} + \frac{\mu_T}{Pr_T}\right]\frac{\partial h}{\partial x_j} \tag{A7}$$

$$\mu_T = \rho k/\omega \tag{A8}$$

$$S_{ij} = \frac{1}{2}\left[\frac{\partial u_i}{\partial x_j} + \frac{\partial u_j}{\partial x_i}\right], \qquad \Omega_{ij} = \frac{1}{2}\left[\frac{\partial u_i}{\partial x_j} - \frac{\partial u_j}{\partial x_i}\right] \tag{A9}$$

The quantities Pr_L and Pr_T are laminar and turbulent Prandtl numbers, respectively. We need just one additional constitutive relation for the k-ω model. Specifically, we assume the Reynolds stress tensor is proportional to the mean strain rate tensor. The resulting relationship is as follows.

Two-equation-model Reynolds stress:

$$\tau_{ij} = 2\mu_T\left[S_{ij} - \frac{1}{3}\frac{\partial u_k}{\partial x_k}\delta_{ij}\right] - \frac{2}{3}\rho k\delta_{ij} \tag{A10}$$

The multiscale model computes each component of the Reynolds stress tensor separately. The model introduces two energy scales corresponding to upper and lower partitions of the turbulence energy spectrum. The quantity ρT_{ij} denotes the upper partition contribution to the Reynolds stress tensor, and ρe denotes the energy of the eddies in the lower partition. The additional equations needed for closure are as follows.

Multiscale model Reynolds stress:

$$\tau_{ij} = \rho T_{ij} - \tfrac{2}{3}\rho e\delta_{ij} \tag{A11}$$

$$\frac{\partial}{\partial t}(\rho T_{ij}) + \frac{\partial}{\partial x_k}(\rho u_k T_{ij}) = -P_{ij} + E_{ij} \tag{A12}$$

$$\frac{\partial}{\partial t}[\rho(k-e)] + \frac{\partial}{\partial x_j}[\rho u_j(k-e)]$$

$$= (1-\hat{\alpha}-\hat{\beta})\,\tau_{ij}\frac{\partial u_i}{\partial x_j} - \beta^*\rho\omega k(1-e/k)^{3/2} \tag{A13}$$

$$E_{ij} = -C_1\beta^*\omega[\tau_{ij} + \tfrac{2}{3}\rho k\delta_{ij}] + \hat{\alpha}P_{ij} + \hat{\beta}D_{ij}$$

$$+ \hat{\gamma}\rho k\left[S_{ij} - \frac{1}{3}\frac{\partial u_k}{\partial x_k}\delta_{ij}\right] + \frac{2}{3}\beta^*\rho\omega k(1-e/k)^{3/2}\delta_{ij} \tag{A14}$$

$$P_{ij} = \tau_{im}\frac{du_j}{\partial x_m} + \tau_{jm}\frac{\partial u_i}{\partial x_m}, \qquad D_{ij} = \tau_{im}\frac{\partial u_m}{\partial x_j} + \tau_{jm}\frac{\partial u_m}{\partial x_i} \tag{A15}$$

Finally, these equations involve a number of closure coefficients whose values are given by the following equations.

Closure coefficients:

$$\beta = {}^3/_{40}, \quad \beta^* = {}^9/_{100}, \quad \sigma = \tfrac{1}{2}, \quad \sigma^* = \tfrac{1}{2} \tag{A16}$$

$$\alpha = [\beta(1 + \hat{\xi}\sqrt{\beta^*}) - \sigma\kappa^2\sqrt{\beta^*}]/\beta^* \tag{A17}$$

$$\hat{\alpha} = {}^{42}/_{55}, \quad \hat{\beta} = {}^6/_{55}, \quad \hat{\gamma} = \tfrac{1}{4} \tag{A18}$$

$$\hat{\xi} = \begin{cases} 0, & k\text{-}\omega \text{ model} \\ 1, & \text{multiscale model} \end{cases} \tag{A19}$$

References

[1]Beam, R. M., and Warming, R. F., "An Implicit Finite-Difference Algorithm for Hyperbolic Systems in Conservation Law Form," *Journal of Computational Physics,* Vol. 22, Sept. 1976, pp. 87–110.

[2]van Leer, B., "Towards the Ultimate Conservative Difference Schemes V. A Second Order Sequel to Godunov's Method," *Journal of Computational Physics,* Vol. 32, July 1979, pp. 101–136.

[3]MacCormack, R.W., "A Numerical Method for Solving the Equations of Compressible Viscous Flow," AIAA Paper 81-0110, Jan. 1981.

[4]Roe, P. L., "Approximate Riemann Solvers, Parameter Vectors, and Difference Schemes," *Journal of Computational Physics,* Vol. 43, Oct. 1981, pp. 357–372.

[5]MacCormack, R.W., "Current Status of Numerical Solutions of the Navier-Stokes Equations," AIAA Paper 85-0032, Jan. 1985.

[6]Jones, W. P. and Launder, B. E., "The Prediction of Laminarization with a Two-Equation Model of Turbulence," *International Journal of Heat and Mass Transfer,* Vol. 15, Feb. 1972, pp. 301–314.

[7]Wilcox, D. C., "Reassessment of the Scale Determining Equation for Advanced Turbulence Models," *AIAA Journal,* Vol. 26, No. 11, 1988, pp. 1299–1310.

[8]Rodi, W. and Scheuerer, G., "Scrutinizing the k-ϵ Turbulence Model Under Adverse Pressure Gradient Conditions," *Transactions of the ASME,* Vol. 108, June 1986, pp. 174–179.

[9]Lakshminarayana, B., "Turbulence Modeling for Complex Shear Flows," *AIAA Journal,* Vol. 24, No. 12, 1986, pp. 1900–1917.

[10]Kolmogorov, A. N., "Equations of Turbulent Motion of an Incompressible Fluid," Izvestiya Academy of Sciences, USSR; Physics, Vol. 6, Nos. 1, 2, 1942, pp. 56–58.

[11]Saffman, P. G., "A Model for Inhomogeneous Turbulent Flow," *Proceedings of the Royal of Society,* London, Series A, Vol. A317, June 1970, pp. 417–433.

[12]Wilcox, D. C., "Multiscale Model for Turbulent Flows," *AIAA Journal,* Vol. 26, No. 11, 1988, pp. 1311–1320.

[13]Sarkar, S., Erlebacher, G., Hussaini, M. Y., and Kreiss, H. O., "The Analysis and Modeling of Dilatational Terms in Compressible Turbulence," Institute for Computer Applications in Science and Engineering, Rept. 89-79, Hampton, VA, 1989.

[14]Zeman, O., "Dilatational Dissipation: The Concept and Application in Modeling Compressible Mixing Layers," *Physics of Fluids A,* Vol. 2, No. 2, Feb. 1990, pp. 178–188.

[15]Wilcox, D. C., *Turbulence Modeling for CFD,* DCW Industries, Inc., La Cañada, CA, 1992.

[16]Rubel, A., and Melnik, R. E., "Jet, Wake and Wall Jet Solutions Using a k-ϵ Turbulence Model," AIAA Paper 84-1523, June 1984.

[17]Kline, S. J.,Cantwell, B. J., and Lilley, G. M., *1980-81 AFOSR-HTTM-Stanford Conference on Complex Turbulent Flows,* Vol. 1, Stanford Univ. Press, Stanford, CA, 1982, p. 368.

[18]Blottner, F. G., "Variable Grid Scheme Applied to Turbulent Boundary Layers," *Computer Methods in Applied Mechanics and Engineering,* Vol. 4, No. 2, Sept. 1974, pp. 179–194.

[19]Settles, G. S., Vas, I. E., and Bogdonoff, S. M., "Details of a Shock Separated Turbulent Boundary Layer at a Compression Corner," *AIAA Journal,* Vol. 14, No. 12, 1976, pp. 1709–1715.

[20]Wilcox, D. C., "Program EDDY2C User's Guide," DCW Industries, Inc., Rept. DCW-R-NC-07, La Cañada, CA, Sept. 1990.

[21]Saffman, P. G., and Wilcox, D. C., "Turbulence-Model Predictions for Turbulent Boundary Layers," *AIAA Journal,* Vol. 12, No. 4, 1974, pp. 541–546.

[22]Cole, J., *Perturbation Methods in Applied Mathematics,* Blaisdell, Waltham, MA, 1968, pp. 106–111.

[23]van Driest, E. R., "Turbulent Boundary Layer in Compressible Fluids," *Journal of the Aeronautical Sciences,* Vol. 18, March 1951, pp. 145–160, 216.

[24]Wilcox, D. C., and Traci, R. M., "A Complete Model of Turbulence," AIAA Paper 76-351, July 1976.

[25]Patel, V. C., Rodi, W., and Scheuerer, G., "Turbulence Models for Near-Wall and Low Reynolds Number Flows: A Review," *AIAA Journal,* Vol. 23, No. 9, 1985, pp. 1308–1319.

[26]Huang, P. G., Bradshaw, P., and Coakley, T. J., "Assessment of Closure Coefficients for Compressible-Flow Turbulence Models," NASA TM-103882, 1992.

[27]Wilcox, D. C., "Supersonic Compression-Corner Applications of a Multiscale Model for Turbulent Flows," *AIAA Journal,* Vol. 28, No. 7, 1990, pp. 1194–1198.

[28]Bardina, J., Ferziger, J. H., and Reynolds, W. C., "Improved Turbulence Models Based on Large Eddy Simulation of Homogeneous, Incompressible, Turbulent Flows," Dept. of Mechanical Engineering, Stanford Univ., Rept. TF-19, Stanford, CA, 1983.

[29]Favre, A., "Equations des Gaz Turbulents Compressibles," *Journal de Mécanique,* Vol. 4, No. 3, 1965, pp. 361–390.